

Investigation of the low-frequency stray current induced corrosion on reinforced concrete infrastructure in high-speed rail transit power supply system

Peng Han^a, Guofu Qiao^{a,b,c,*}, Bingbing Guo^d, Dongsheng Li^e, Jinping Ou^a

^a School of Civil Engineering, Harbin Institute of Technology, Harbin 150090, China

^b Key Lab of Smart Prevention and Mitigation of Civil Engineering Disasters of the Ministry of Industry and Information Technology, Harbin Institute of Technology, Harbin 150090, China

^c Key Lab of Structures Dynamic Behavior and Control of the Ministry of Education, Harbin Institute of Technology, Harbin 150090, China

^d School of Civil Engineering, Xi'an University of Architecture and Technology, Xi'an 710055, China

^e School of Civil Engineering, Dalian University of Technology, Dalian 116024, China

ARTICLE INFO

Keywords:

Stray current
Corrosion
Reinforced concrete infrastructure (RCI)
Quasi-steady state
Oxygen

ABSTRACT

High-speed electrified rail transit (HSERT) has been developed intensely worldwide. However, the reinforced concrete infrastructure (RCI), especially for the deck of viaducts, has the risk of stray current (SC) induced corrosion. The present research is dedicated to revealing the mechanism of low-frequency SC (LSC) induced corrosion and providing a scientific basis to ensure serviceability, sustainability and cycle-life performance design of RCI. Considering the spatial distribution and time consumption of oxygen as well as pore saturation of RCI, the mathematical model of LSC induced corrosion is established. Based on the fluctuations of oxygen concentration, the quasi-steady state is proposed. And the corrosion behaviors of RCI with different pore saturation subjected to LSC are compared systematically. The results of mathematical model are verified by the measurement of half-cell potential.

1. Introduction

The rapid development of the high-speed electrified rail transit (HSERT) meets the strategic requirements of energy conservation, environmental protection and sustainable development, which has gradually become one of the most vital modes of transportation for individuals. The reinforced concrete infrastructures (RCI), especially for the viaducts, play a significant role in the safety of HSERT. However, corrosion induced by stray current (SC) from HSERT seriously affecting the durability of RCI[2].

The SC is prescribed for the current which is not returned to the substation through designed path (running rail) in electric traction system. The path of SC composed of the concrete and the reinforced steel which act as the electrolyte and electrode in the electrochemical corrosion system. It has been conclusively demonstrated that the electrochemical behavior of adjacent RCI will be disturbed obviously by SC [3-7]. The electrified rail network of HSERT, in the UK, comprises 600

V/750 V direct current (DC) and 25 kV (50 Hz) alternating current (AC) power[5]. Nevertheless, even in a DC power supply system, the actually monitored SC is not in DC form. Peabody[8] monitored the fluctuations of pipe potential (vs. CSE) versus time among one day, and low frequency and bipolarity potential characteristic of pipe subjected to SC can be inferred from his report. Similar results have been obtained by Charalambous[9] and Xu[10]. Thus, low-frequency stray current (LSC) is an important part of SC. However, the DC induced corrosion has been widely studied[1,11-16], but AC still has been a largely under explored domain.

Periodic or non-periodic transient electrochemical processes are more complex relative to DC induced corrosion due to the multifactorial traits of AC, e. g. frequency, amplitude and bias voltage. Bertolini[17] evaluates that AC-current induced corrosion is less dangerous than DC. But obvious macrocell corrosion can be observed in chloride-contaminated concrete under AC-current (50 Hz). Reinforced concrete structure contaminated by chloride salts are common in civil engineering, such as the roads which is sprayed with deicing salt in winter and

* Corresponding authors at: School of Civil Engineering, Harbin Institute of Technology, Harbin 150090, China.

E-mail addresses: hanpeng_0914@163.com (P. Han), qgf_forever@hit.edu.cn (G. Qiao), guobingbing212@163.com (B. Guo), lidongsheng@dlut.edu.cn (D. Li), oujinpjng@hit.edu.cn (J. Ou).

<https://doi.org/10.1016/j.ijepes.2021.107436>

Received 7 January 2021; Received in revised form 12 June 2021; Accepted 18 July 2021

Available online 27 July 2021

0142-0615/© 2021 Elsevier Ltd. All rights reserved.

Nomenclature	
E_{app}	Applied potential between positive and negative electrode (V)
E_p	The amplitude of AC voltage (V)
f	The frequency of AC voltage (Hz)
c_i	Concentration of i ion (mol/m^3)
J_i	The flux of species i ($\text{mol}/(\text{m}^2\cdot\text{s})$)
D_i	The diffusion parameter of oxygen, $8 \times 10^{-10} \text{ m}^2/\text{s}$ for saturated mortar and $8 \times 10^{-9} \text{ m}^2/\text{s}$ for 40% pore saturated mortar[1]
z_i	The number of electrons
$u_{m,i}$	Mobility of species i ($\text{s}\cdot\text{mol}/\text{kg}$)
F	The Faraday constant, 96,485 (C/mol)
ϕ_l	The electrolyte potential (V)
ϕ_s	The electrode potential (V)
\mathbf{v}	The velocity vector (m/s)
R	Gas constant, 8.314 J/(mol·K)
T	Temperature, 293.15 (K)
ρ	Electric charge density (C/m^3)
\mathbf{i}_l	The electrolyte current density vector (A/m^2)
\mathbf{i}_s	The electrode current density vector (A/m^2)
$\sigma_{l/s}$	σ_l : The electrolytic conductivity (S/m), 0.01 S/m for saturated mortar and 0.003 S/m for 40% pore saturated mortar/ σ_s : The electrode conductivity (S/m), 4.032×10^6 (S/m)
	E_0^{Fe} Standard electrode potential of iron (V vs. SHE)
	$E_0^{O_2}$ Standard electrode potential of oxygen (V. vs. SHE)
	ΔG Gibbs free energy (kJ/mol)
	$E_{eq,a/c}$ Equilibrium potential (V), the subscripts 'a' for anode and 'c' for cathode
	Δm Corrosion weight loss (g)
	i_a The anode corrosion current density (A/m^2)
	$i_{0,a}$ The anode exchange current density (A/m^2)
	i_c The cathode corrosion current density (A/m^2)
	$i_{0,c}$ The cathode exchange current density (A/m^2)
	$A_{a/c}$ The anode/cathode Tafel slope (V/dec)
	K_a^0 Reaction rate constant
	c_{bulk} The concentration of bulk solution, 0.28 (mol/m^3)
	$c_{interface}$ The concentration of interface solution (mol/m^3)
	E_{cor}/i_{cor} The self-corrosion potential (V)/The self-corrosion density (A/cm^2)
	E_{half} The half-cell potential (V. vs. ref)
	η Overpotential (V. vs. ref)

the building structure adjacent to coastal areas. Lavani[18,19] demonstrated that the AC-induced corrosion is related to the peak voltage of the applied signal as well as the ratio of the anode and cathode Tafel slope. And time average and root-mean-square current are proposed as indicators to describe the faraday and non-faraday process. Tang[20] presented the AC-induced corrosion degree under 30 mA (50 Hz) anode polarization for a certain time, and then several electrochemical methods (Tafel polarization test, cyclic potentiodynamic polarization (CP) test and electrochemical impedance spectroscopy (EIS)) are employed to demonstrate the corrosion degree. And corrosion related equations under AC disturb are proposed and solved based on the equivalent electrical circuit model. Besides, it is acknowledged that the real-time monitoring of corrosion subjected to the SC is also critical for the performance-based design of RCI and the optimization of corrosion protection systems. But from the perspective of cost and technology, there are still certain challenges in achieving accurate real-time corrosion monitoring. The transient numerical simulation method, currently, seem to be an alternative implementation method. Hong[2] developed a finite element method (FEM) to present the corrosion characteristics of viaduct subjected to SC which is regarded as a form of DC. Meanwhile, intensive, dynamic and local corrosion characteristics were summarized. Nevertheless, the LSC, obviously, is more consistent with engineering. Furthermore, considering the multiple issues such as depolarizers can make the model more universal. Ouadah[6] diagnosed that electromagnetic induction significantly affects the electrochemical behavior and accelerates the corrosion rate of steel. Zhu[21] indicated that the corrosion susceptibility increases with decreasing AC frequency (30–1000 Hz). In summary, the existing research mainly focuses on the corrosion evaluation of high-frequency AC or DC[22–25], and the research on the low-frequency AC considering multifactorial processes which satisfy the characteristic of SC is still insufficient. And the related transient numerical simulation methods still should be further improved.

A host of issues affect LSC induced corrosion need to be considered. Firstly, the passivation film, formed around the surface of reinforced due to alkaline environment provided by the hydration of the clinker, can be destroyed by the existed or introduced chloride (from aggressive environment) ions in RC[26,27]. Mundra[28] developed a constant value of $[\text{Cl}]/[\text{OH}]^3$, which can be employed to predict of the onset of pitting, interlinking chloride concentration and the solubility of the passive film

in simulated pore solution of low-Ca alkali-activated concrete via a range of electrochemical techniques. Besides, in Mundra' s recent research[29], a model of chloride ingress into alkali-activated slags was proposed based on thermodynamic calculations (chloride binding capacity and porosity of the binder). All the above studies have proved the potential threat of chloride induced corrosion, especially the damage of the passive film. Secondly, the electrochemical corrosion process is fully affected by the distribution and the species of depolarization agent which mainly composed of oxygen[1,30]. Thirdly, the path of SC determined by the resistivity of RCI (pore saturation) is also a crucial condition[31].

In summary, the research on corrosion failure caused by the LSC is still insufficient to provide enough scientific basis for engineering. The contents of this paper are conducted as follows: Section two starts by laying out the corrosion-related partial differential equations (PDE) and boundary conditions. The third section concerns with the electrode process kinetics parameters via electrochemical methods (Tafel). The fourth section presents and interprets the results of the numerical simulation, focusing on several factors affect the LSC-induced corrosion. The proposed numerical results are consistent with experimental data. We conclude the investigation in Section 5.

2. Mathematical model of LAC SC-induced corrosion

2.1. Geometry model of the RCS

The current of rail transit, generally, comes from the rail transit power system and back to substation via the running rail as designed. However, possible defects and inevitable aging of the insulating material between rails and ground lead to the formation of SC. RCI is the major materials subjected to SC, and reinforcement cage, as the crucial return path of SC, is disturbed significantly. Indeed, the spatial distribution of reinforcement is a common condition which has considerable impact on electrochemical characteristics. Nevertheless, on the one hand, the kinetics parameters of the electrode processes at the steel–concrete interface, in general, are the primary cause of the above difference. On the other hand, for reinforced concrete structures or members, compare with that of the natural corrosion, the significant features of the SC-induced corrosion are local, dynamic and intensive. The anode and cathode regions, which seriously threaten the durability of the structure,

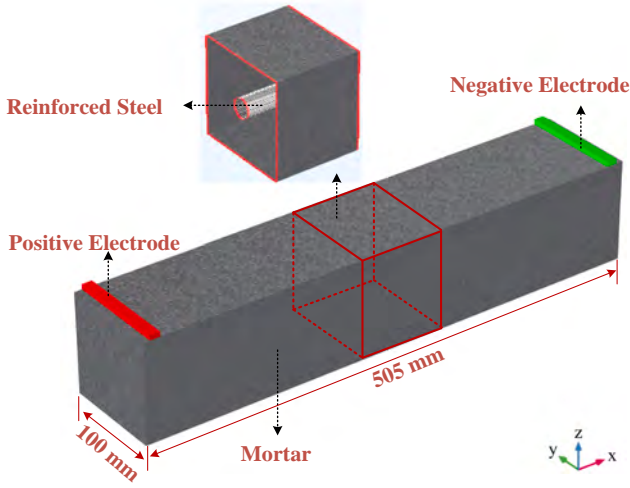


Fig. 1. Simplified 2D geometry model of RCS.

are distributed near the injection and extraction points of SC. Thus, a simplified geometry model (see Fig. 1), in present research, is employed instead of structures or members, focusing on the corrosion behavior of anode and cathode regions. Besides, the use of small specimens has the following merits: saving computing resources, higher model convergence, more accurate verification tests and strong repeatability. The established model is also able to extended to structures or members.

Fig. 1 lays out the simplified RCI composed of a mortar (100*100*505 mm), a reinforced steel ($\phi 20$ mm) and two electrodes (graphite, 10*5*100 mm). Voltage signal is applied between positive and negative electrode to simulate the orbital voltage drop. Also, the positions of the electrode are assumed to be the region of weak insulation which observed frequently and commonly adjacent to the welding points and substation area.

2.2. Numerical model of LAC-SC-induced corrosion

As mentioned in section 1, low frequency and bipolarity electrode potential characteristic subjected to SC have been monitored. Furthermore, X. L. Zhang[32] reported that the influence of the charge–discharge process of electric double layer on the electrochemical test system can be gradually ignored as the rate of the potential change (scan rate) decreases. In present research, the frequency of 0.001 Hz of AC signal was adopted to explore the LSC-induced corrosion in several electrode process, which meets the characteristic of SC[8-10], and the influence of charge–discharge process on faraday process is neglected due to the extremely low frequency.

In order to make the electrode potential fluctuate sinusoidally at above frequency, AC signal, which governed by Eq. (1), was applied between positive and negative electrode as shown in Fig. 2. Obviously, the potential fluctuation of the electrode (reinforcement) subjected to SC is frequently non-periodic, the hypothesis of periodic fluctuation, however, is acceptable to initially reveals the corrosion mechanism of LAC-SC in present research.

$$E_{app} = E_p \sin(2\pi ft) \quad (1)$$

Electrochemical corrosion occurs at the electrolyte–electrode interface. Thus, partial/ordinary differential equations and boundary conditions should be defined at electrolyte, electrode and electrolyte–electrode interface based on the physics and chemical process, respectively. The chloride ion acts as the catalysts during the process of steel corrosion. It can be inferred that the migration phenomenon of chloride caused by SC will not be obvious due to the period electric signals. Adversely, oxygen, which is the primary depolarization agent, is consumed rapidly due to the LAC-SC, thereby, the diffusion of oxygen in concrete should be taken into consideration. The influences of the concentration of chloride are presented via the parameters of the electrode kinetics process.

The diffusion of oxygen is governed by the Fick's second law as listed below:

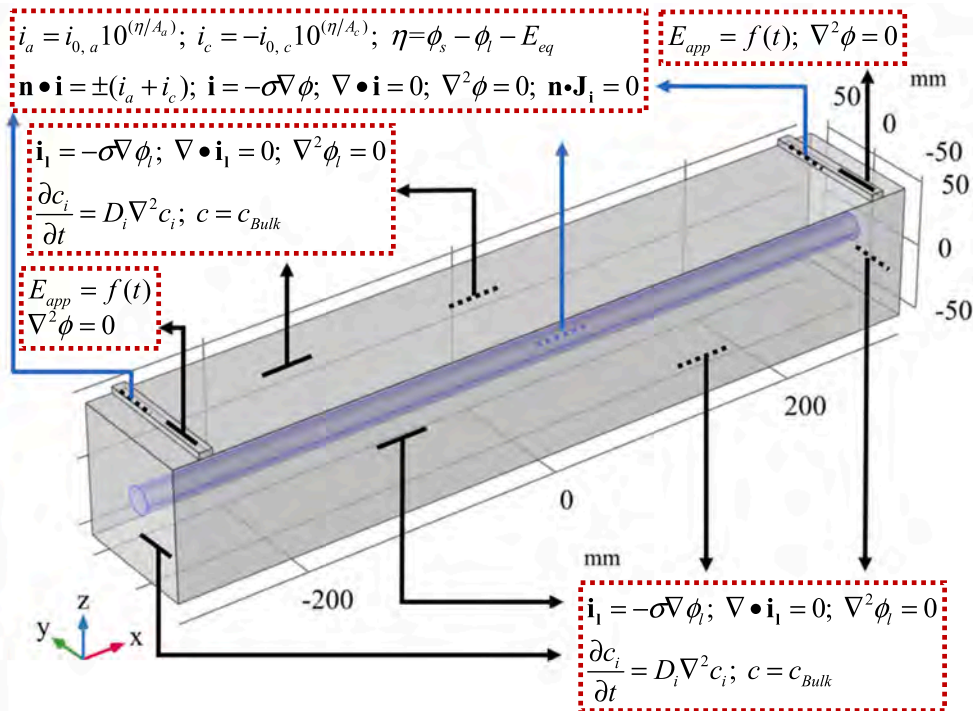


Fig. 2. The schematic diagram of the position where equations and boundary conditions are applied.

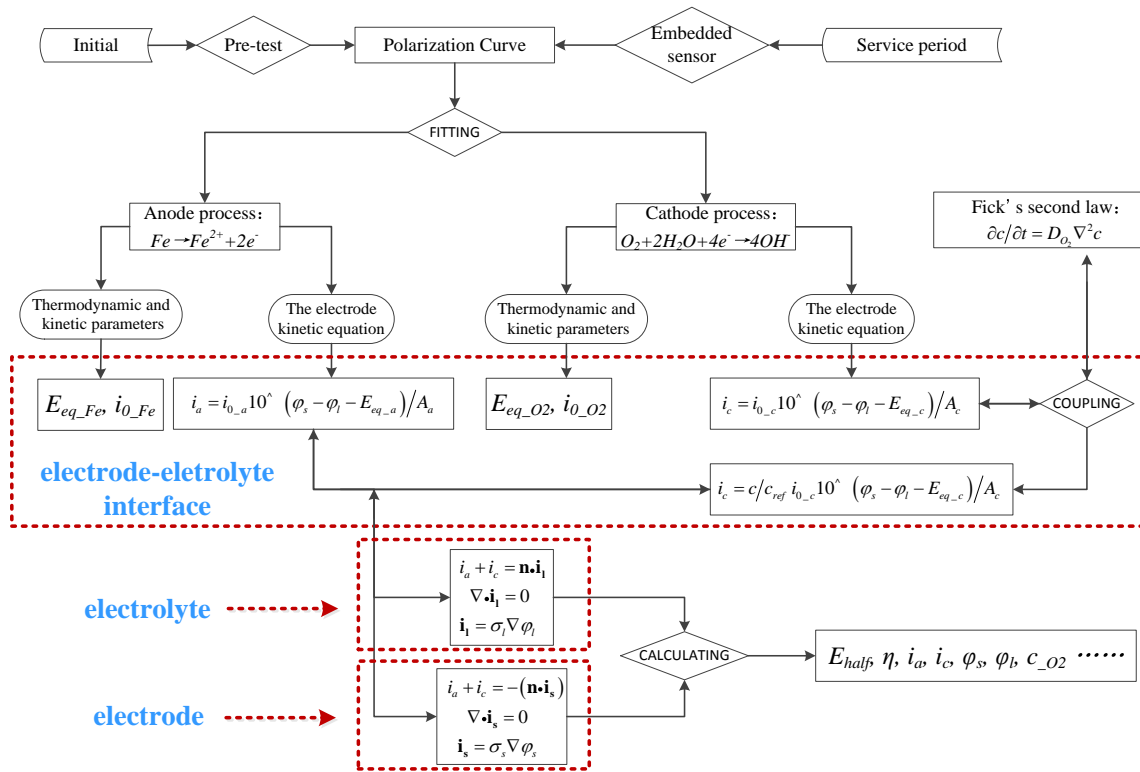


Fig. 3. The flow chart of the detailed modeling process.

$$\frac{\partial c_i}{\partial t} = -\nabla \cdot \mathbf{J}_i \quad (2)$$

$$\mathbf{J}_i = -D_i \nabla c_i - z_i u_{m,i} F c_i \nabla \phi_l + \mathbf{v} c_i \quad (3)$$

$$u_{m,i} = \frac{D_{m,i}}{RT} \quad (4)$$

The above equations take account the individual transport of charged and uncharged species in concrete via diffusion, migration and convection. As mentioned above, the only species considered in present research is the oxygen, thus, the Eqs. (2)–(4) can be simplified as Eq. (5):

$$\frac{\partial c_i}{\partial t} = D_i \nabla^2 c_i \quad (5)$$

where i corresponds to the oxygen. D_i is the oxygen diffusion parameter which is closely related to the pore saturation of the mortar. The concentration of dissolved oxygen is determined by the thermodynamic calculations (Henry's law), which is mainly influenced by the temperature and partial pressure. As shown in Eq. (6), 'SI' stands for saturation index, 'f' refers to the fugacity depend on partial pressure of oxygen, 'a' represents the activity of dissolved oxygen in electrolyte solution and 'K' denotes the equilibrium constant (Henry constant) which is determined by temperature and obtained from thermodynamic database (CEM-DATA18.dat[35]). The calculated dissolved oxygen concentration (approximately equal to dissolved oxygen activity due to the relatively low ionic strength in present research), at 1 atm (0.21 partial pressure) and 20 °C, is 0.286 mol/m³, which is employed as the initial value in present research.

$$SI = \lg(f) = \lg \frac{a}{K} \quad (6)$$

$$\frac{\partial \rho}{\partial t} + \nabla \cdot \mathbf{i}_{s/l} = 0 \quad (7)$$

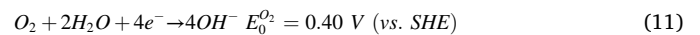
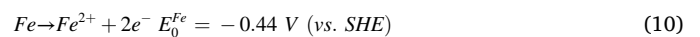
The described electrochemical cell obeys the current conservation Eq. (7). The divergence of current density vector demonstrates that the

amount of charge flowing out of the unit volume in an infinitely small unit. For presented electrochemical cell, the partial derivative of the charge density in arbitrary points equal to zero. Thus, the divergence of current density vector equal to zero. Ohm's law (see Eq. (8)) is used in combination with the current conservation to interpret the flow of currents. Finally, Laplace's equation was obtained (see Eq. (9)).

$$\mathbf{i}_{s/l} = -\sigma_{s/l} \nabla \phi_{s/l} \quad (8)$$

$$\nabla^2 \phi_{s/l} = 0 \quad (9)$$

In the alkaline environment of concrete, the semi-reaction of the anode process is mainly the oxidation of iron (see Eq. (10)). Meanwhile, the majority of cathode process is reduction of oxygen (see Eq. (11)).



From the view of thermodynamics, the imperative conditions for judging whether the electrode reaction can occur spontaneously is that the Gibbs free energy required is less than zero (see Eq. (12)), meanwhile reaching the activation free energy barrier. Eqs. (10) and (11) are the spontaneous electrode reaction. The standard hydrogen potential is a crucial indicator for judging the occurrence of a reaction.

$$\Delta G = nFE_0 \quad (12)$$

From the perspective of electrode kinetics process, overpotential (see Eq. (13)), defined by the difference among electrode, electrolyte and equilibrium potential, is one of the criteria for evaluating electrode reaction rate. Derived from the Faraday's laws, the current density is proportional to the electrode reaction rate as described in Eq. (14). The Tafel equations are adopted to estimate the anode and cathode electrode reaction current density (see Eq. (15)).

$$\eta = \phi_s - \phi_l - E_{eq,a/c} \quad (13)$$

$$\Delta m = \frac{Mi_a t}{nF} \quad (14)$$

$$i_a = i_{0,a} 10^{(\eta/A_a)}; i_c = -i_{0,c} 10^{(\eta/A_c)} \quad (15)$$

where $i_{0, a/c}$ corresponds to the anode and cathode exchange current density. The anode process is assumed to be controlled by the charge transfer, and the cathode is diffusion control. However, the oxygen concentration is defined as constant in the expression of $i_{0, c}$ as shown in Eq. (16). Modification, thus, should be introduced to accurately calculate the cathodic reaction. Based on the phenomenon of the oxygen diffusion phenomenon described by Fick's second law, the bulk concentration adopted in Eq. (16) should be replaced by interface concentration as shown in Eq. (17).

$$i_{0,c} = nFK_a^0 c_{bulk} \quad (16)$$

$$i_{0,c} = nFK_a^0 c_{interface} \quad (17)$$

The current density of steel–concrete interface can be expressed as Eqs. (18) and (19). The boundary of concrete is governed by the condition of insulation and no flux as shown in Eqs. (20) and (21). In addition, the concentration boundary is defined on every outer surface of the concrete (see Eq. (22)).

$$n \cdot i_l = i_a + i_c \quad (18)$$

$$n \cdot i_s = -(i_a + i_c) \quad (19)$$

$$n \cdot i_l = 0; n \cdot i_s = 0 \quad (20)$$

$$n \cdot J_i = 0 \quad (21)$$

$$c = c_{bulk} \quad (22)$$

The applied positions of all above equations and boundary conditions in electrochemical cell are shown in Fig. 2. The flow chart of the detailed modeling process is illustrated in Fig. 3. The polarization curve describing the reaction kinetics process, in present research, is obtained via the pre-test depicted in Section 3.2. As the service time of the structure increases, the embedded corrosion sensors, which have been reported in our previous works[33,34], can be used to monitor the reaction kinetics characteristics and revised the kinetics parameters obtained by pre-test in present research.

The finite element method (FEM) is adopted to solve the equations via COMSOL MULTIPHYSICS. The ‘Tertiary current Distribution, Nernst-Planck’ physics in COMSOL has been adopted to describe the electrode, electrolyte and the electrode–electrolyte interface. For electrode and electrolyte, the current conservation and Ohm’s law are defined; Besides, the Fick’s second law is employed to describe the transport of oxygen in electrolyte. For electrode–electrolyte interface, the reaction kinetics processes are proposed via Tafel empirical equations. The cathode kinetics process is coupled with the transport of oxygen. The relationship among the electrode, electrolyte and electrode–electrolyte interface current density are realized through the definition of current density as shown in Eqs. (18) and (19). The ‘Time Dependent’ study in COMSOL has been employed due to the description of the oxygen transport process. The time step is set to 20 s. The mesh of the model includes 40,273 domain elements, 4084 boundary elements and 768 edge elements. Also, the interface of electrode and electrolyte is encrypted for more accurate analysis of variables.

3. Materials and experiments

3.1. The materials of experiments

The cement-based material adopted in present research is mortar specimen which composed of cementitious materials, fine aggregates,

Table 1
The proportion of mortar specimen (kg/m³).

Cement	Sand	Water	Water-cement ratio
585	1758	293	0.5

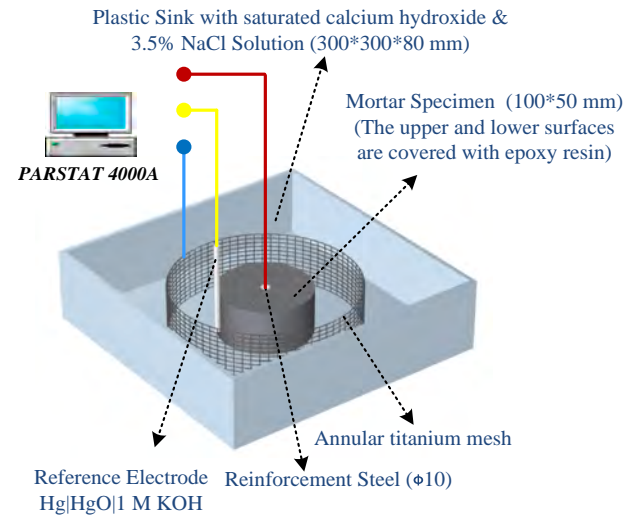


Fig. 4. The schematic diagram of electrochemical test device based on the three-electrode system.

water and corrosive ions introduced. The proportion of mortar specimen is shown in Table 1. Ordinary Portland Cement of 42.5 MPa and medium sand of region II are adopted. The content of corrosive ions (Cl⁻) in the mass fraction of cementitious materials are set as 3.0%.

The hot rolled plain steel of Q235 are employed in present research. The surface of steel is polished via 100#, 360#, 500#, 800#, 1500# and 2000# sandpaper, respectively. Graphite is employed as the positive and negative electrodes.

3.2. Electrochemical test

The Tafel polarization test (TPT), with IR compensation, on the one hand, is employed to demonstrate the corrosion characteristic of RCI within two pore saturation (40% and 100%) mortar, on the other hand, to come up with kinetics parameters for FEM as boundary conditions.

TPT is to polarize ± 250 mV, with 0.1667 mV/s scan rate, in both positive and negative directions relative to the open circuit potential (OCP) of the working electrode. And the kinetics parameters are obtained via linear extrapolation from Tafel region. Furthermore, the TPT is conducted via three electrode system with PARSTAT 4000A ELECTROCHEMICAL WORKSTATION. Considering the exposed surface of the working electrode and counter electrode, the test device as shown in Fig. 4 has been employed, the upper and lower surfaces of mortar are sealed with epoxy resin. The work electrode (WE) is reinforced steel mentioned in Section 3.1, which has a diameter of 10 mm and a height of 50 mm. Mercuric oxide electrode (Hg|HgO|1 M KOH) with double electrolytic bridge is adopted as reference electrode (RE). The standard electrode potential is 0.098 V at 25 °C (All potentials involved in present research are versus Hg|HgO|1 M KOH). Titanium mesh plate was employed as auxiliary electrode (counter electrode (CE)).

3.3. Half-cell potential test

Half-cell potential method can rapidly, preliminary and qualitatively monitor the degree of corrosion induced by SC via observing the potential variation which is widely adopted in engineering. The saturated copper sulfate electrode (Cu|CuSO₄ (saturated)) is adopted as RE. The

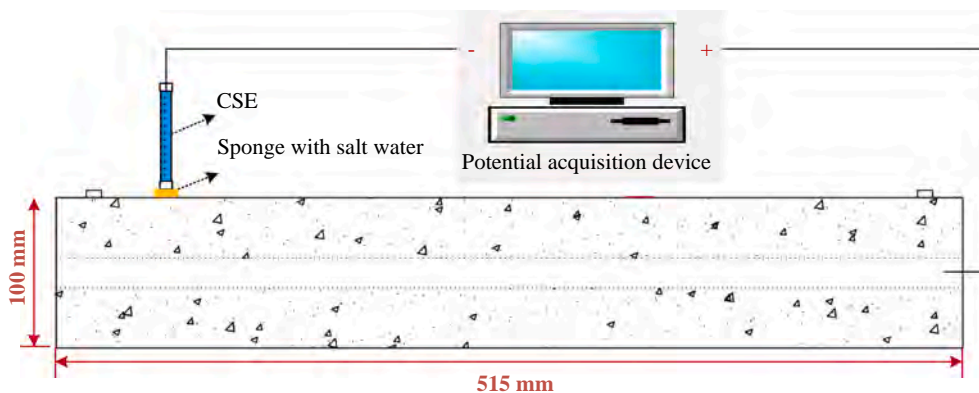


Fig. 5. The schematic diagram of half-cell potential monitor device.

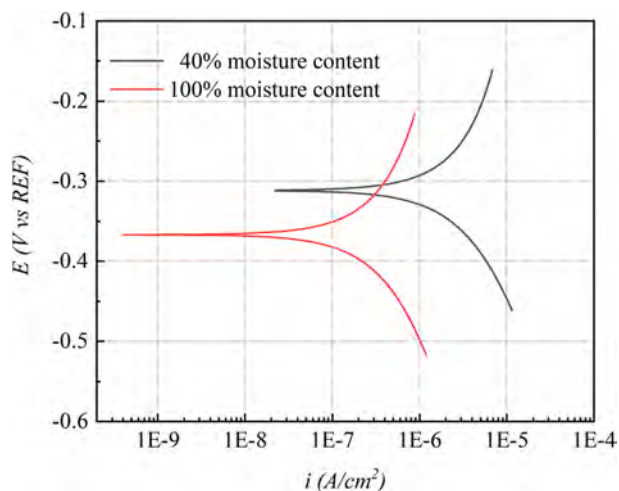


Fig. 6. Polarization plot; 3% NaCl under 40% and 100% moisture content of mortar.

standard electrode potential is 0.316 V at 25 °C. The positive and negative electrodes of the potential acquisition device is connected to the reinforced and reference electrode respectively. The schematic diagram of the experimental device is shown in Fig. 5.

4. Results and discussion

4.1. Tafel test results

Fig. 6 presents the Tafel plot under the 100% and 40% pore saturated mortar. The mortar, with low moisture content, is located at the upper right of plot, corresponding to a higher corrosion rate. It can be inferred that the moisture content seems to be a crucial condition to determine the corrosivity. Besides, the concentration of the depolarizer (oxygen) dissolved in pore solution and the diffusion parameters in the mortar are the general issues affecting corrosion. As the pore saturation of mortar is low, the diffusion resistance of oxygen is narrow, and the oxygen consumed by the cathode process can be rapidly replenished. However, the necessary condition for the electrochemical reaction is the presence of electrolyte solution. Therefore, it is not that the lower the pore saturation, the greater the corrosiveness of the mortar.

The kinetics parameters (E_{cor} , i_{cor} , B_a and B_c) obtained by the linear extrapolation method based on the electrochemical theory are illustrated in Table 2. The self-corrosion potential (E_{cor}), with low pore saturation, is higher, but the corresponding self-corrosion current density (i_{cor}) is greater. It seems that the obtained current and potential are contradictory as corrosion evaluation indicators. The self-corrosion

Table 2

The fitting parameters of Tafel polarization curve.

$\omega\%$	E_{cor}/V	$i_{cor}/A/cm^2$	B_a/mV	B_c/mV
100%	-0.367	7.56×10^{-7}	717.22	-441.53
40%	-0.312	6.23×10^{-6}	861.06	-373.98

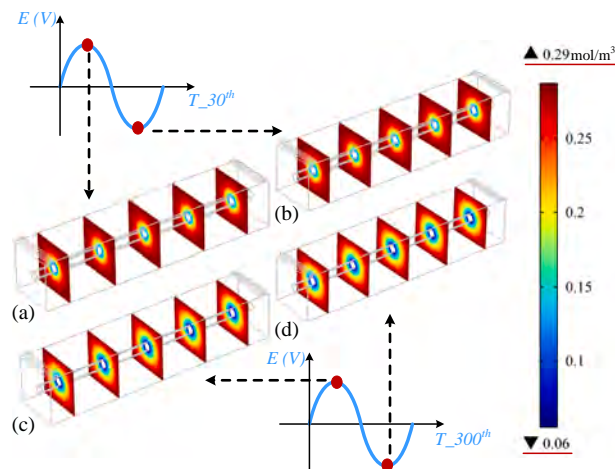


Fig. 7. The distribution of the peaks and troughs of the oxygen concentration within the 30th and 300th AC period in 40% moisture content mortar; (a) the peak of 30th period; (b) the trough of 30th period; (c) the peak of 300th period; (d) the trough of 300th period.

current density (i_{cor}), as a kinetics parameter, is proportional to the corrosion rate, which is the most direct and accurate index for evaluating corrosion behavior in non-polarization state of the electrode. However, the self-corrosion potential (E_{cor}), as a thermodynamic indicator, can only make a preliminary and rough judgment of the corrosion trend.

4.2. Numerical implementation

4.2.1. The variation of corrosion-related physical characteristics in time domain

Fig. 7 exhibits the distribution of the oxygen concentration at a specific time (30th and 300th periods) in mortar with 40% pore saturation. The distribution of saturated mortar is similar and therefore not presented here. Obviously, the oxygen, as the main depolarizer of the cathode, is consumed along the radial direction of the reinforced and replenished at the mortar boundary. The oxygen concentration around the reinforced in 300th period is significantly lower than that in 30th.

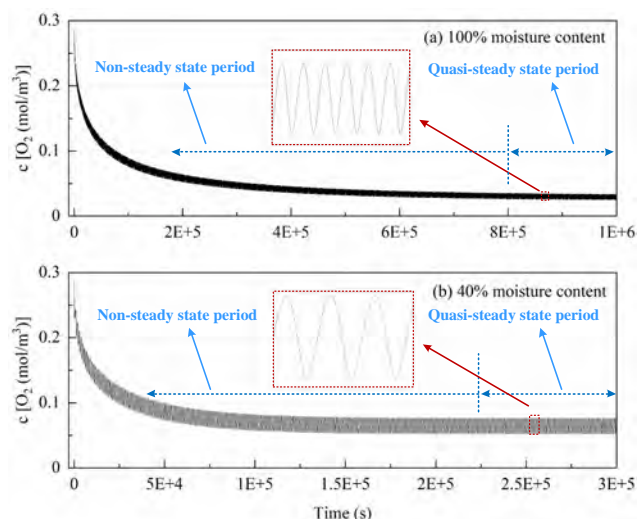


Fig. 8. The fluctuation of oxygen concentration versus time at the point (-202.5 mm, 0 mm, 10 mm); (a) 100% moisture content; (b) 40% moisture content.

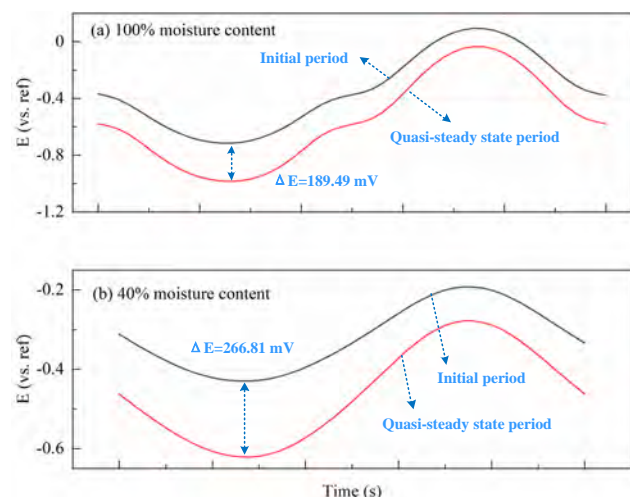


Fig. 9. The half-cell potential in initial period and quasi-steady state period; (a) 100% moisture content; (b) 40% moisture content.

The remarkably changes can be observed within the time domain which not only affects the cathode process, but also induces corresponding disturbances to the entire electrochemical process. Thus, to explore the corrosion mechanism, it is necessary to understand the fluctuation of oxygen in the time domain.

In order to acquire the variation of oxygen versus time at the reinforced interface, a characteristic point (-202.5 mm, 0 mm, 10 mm) is employed, which is located in the area where the concentration fluctuates the most as manifested in Fig. 8. The curve presents a rapid decline and then gradually stabilizes. In the initial stage of AC-SC intervention, the oxygen required for the reaction is still sufficient. The process that oxygen consumption is greater than supplementation. And then, with the gradual consumption of oxygen, the cathode reaction is weakened. Finally, the dynamic equilibrium of two processes are established which may correspond to the solution in the frequency domain. However, on the one hand, the solution of the frequency-based equations are still not perfect, on the other hand, the solution of frequency-based cannot obtain the deviation degree of physical quantity which is pivotal for evaluating the corrosion. Thus, a quasi-steady state, based on oxygen fluctuation characteristics, is defined in time domain as

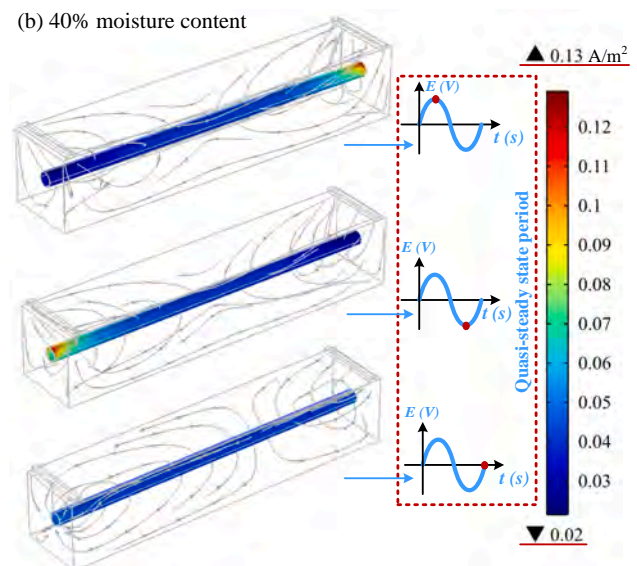
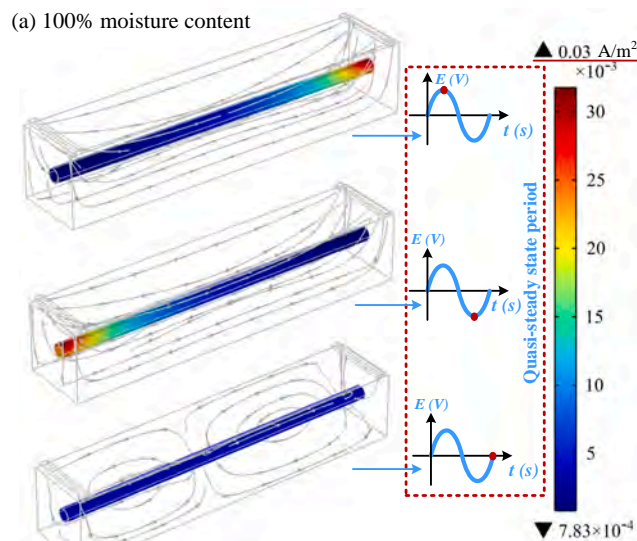


Fig. 10. The corrosion current density plot in quasi-steady period; (a) 100% moisture content; (b) 40% moisture content.

marked in Fig. 8. Compare to the steady-state with infinite time, the differences in physical quantities can be approximately ignored within adjacent periods in quasi-steady state.

It can be acknowledged that the emergence of the quasi-steady state takes longer in saturated mortar. Besides, the concentration and amplitude are lower than that of 40% pore saturated mortar. Obviously, the above phenomenon is probably due to the low diffusion resistance of oxygen in mortar at lower pore saturation, and the new thermodynamic balance is established faster.

4.2.2. The variation of corrosion indexes in quasi-steady state

The half-cell potential is the most commonly used method in engineering to quickly evaluate corrosion. Fig. 9 compares the half-cell potential at initial period (non-steady state) and quasi-steady period with 40% pore saturated and saturated mortar respectively. Obvious potential drop (189.49 mV and 266.81 mV) can be observed from initial to quasi-steady period which also increases the probability of hydrogen embrittlement of reinforced.

The reason for the potential drop is due to the insufficient oxygen

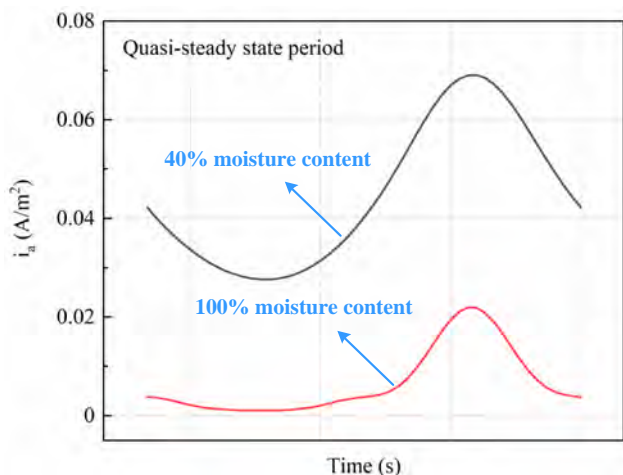


Fig. 11. The corrosion current density within a period in quasi-steady state at the point (-202.5 mm, 0 mm, 10 mm).

content, which leads to the accumulation of electrons in cathode region. On the one hand, greater driving force for the reduction of oxygen is provided, on the other hand, with the continuous decrease of the potential, the Gibbs free energy for the reduction of water is satisfied, and water (pore solution) participates in the cathode process as another depolarizer.

Nevertheless, potential is a thermodynamic parameter which cannot evaluate the electrochemical behavior of different systems quantitatively. According to the faraday law, corrosion current density is proportional to the corrosion rate. Therefore, the distribution and value of corrosion current density are crucial indicators for evaluating the corrosivity of mortar subjected to AC-SC under vary service life.

Fig. 10 demonstrates the distribution of corrosion current density on the surface of reinforced and the direction of electrolyte current in 40% pore saturated and saturated mortars. The characteristic of AC-SC-induced corrosion can be summarized as the following two points:

Firstly, corrosion occurs at the end of the reinforced, which is actually the region where SC flows out. Correspondingly, the strong cathodic reaction probably happens in the injection region of SC. Secondly, the anodic region varies with the fluctuation of AC-SC. It can be inferred that anode and cathode processes alternate in same region. Furthermore, for RC infrastructure, the path of the SC composed of concrete and reinforced. It can be seen from the stream line in Fig. 10 that the SC is more likely to flow back from the reinforced to negative electrode at low pore saturated mortar, which causes significant interference to the electrochemical behavior of reinforced.

In saturated mortar, the maximum corrosion current density is 0.03 A/m². Correspondingly, 0.13 A/m² in 40% pore saturated mortar which is more corrosive. In order to more clearly compare the corrosivity of mortars subjected to AC-SC under two conditions, the corrosion current density of a selected point (-202.5 mm, 0 mm, 10 mm) in quasi-steady state for one period is compared as illustrated in Fig. 11. In saturated mortar, the average corrosion current density in one quasi-steady period is 6.67 mA/m², and it is 44.64 mA/m² in 40% pore saturated mortar. Besides, the fluctuations, in the saturated mortar, in the first half of period are relatively gentle, while the latter half has a large increase. However, the corrosion current density in unsaturated mortar also has a larger drop in first half period. On the one hand, the resistivity of saturated mortar is low, and the half-cell potential is more negative (as discussed in Section 4.2.2); on the other hand, the obtained kinetics parameters (self-corrosion current density) is smaller. Thus, the above reasons lead to the fluctuations characteristics as manifested in Fig. 11.

4.3. Experimental verification

Half-cell potential method is employed to verify the accuracy of mathematical model in present research. In this section, the mortar with 40% pore saturation is adopted as the experimental object to monitor the half-cell potential in the quasi-steady state. And the collected potential relative to copper sulfate electrode has been converted to the mercury oxide electrode. Furthermore, the mortar suffered AC-SC has a potential drop not only in the length but also in the radial direction. Since the reference electrode can only be placed on the surface of the

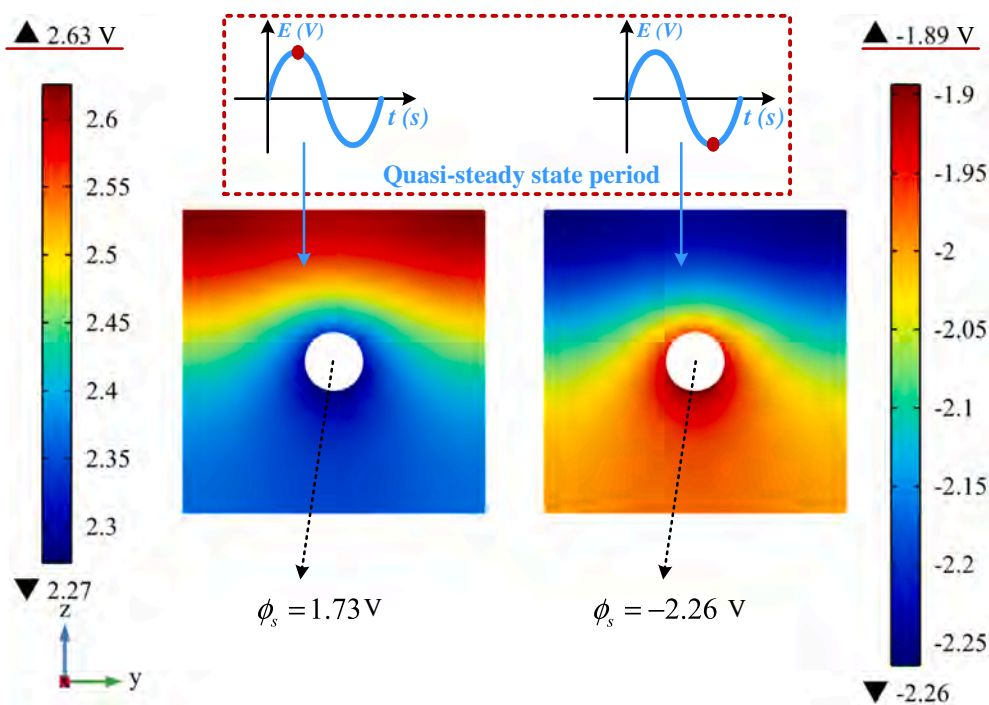


Fig. 12. Distribution of electrolyte potential (ϕ_e) obtained from numerical simulation on cross section of RC ($x = -200$ mm, the coordinates of the geometric model are shown in Fig. 2).

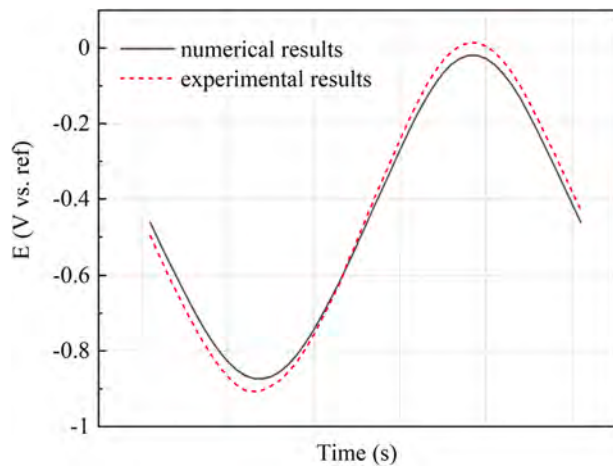


Fig. 13. The half-cell potential of numerical and experimental results at the point (-200 mm, 0 mm, 50 mm) in quasi-steady period.

mortar, the measured half-cell potential actually contains the IR potential from the mortar protective layer and the potential from interface. However, the half-cell potential obtained from numerical simulation is the interface potential. Therefore, the electrolyte potential distribution in the radial direction obtained from numerical simulation is illustrated in Fig. 12. Thereby, IR compensation is performed on the calculated half-cell potential, so as to be consistent with the actual measurement. It can be observed from Fig. 13 that the numerical result (including IR potential) presents good agreement with experiment data.

5. Conclusion

The SC has become a potential hazard deteriorates the durability of RCI due to the rapid development of HSERT. The present research is dedicated to revealing the corrosion mechanism of SC and providing basis for subsequent researches (including the evaluation of serviceability, sustainability and cycle-life performance design of RCI as well as the optimization of corrosion protection system). On the one hand, the LSC which is closer to the actual project is adopted; on the other hand, the spatial distribution and time consumption of oxygen concentration (as the crucial depolarizer for cathode process) as well as the pore saturation of the mortar are considered in FEM. The main conclusions are as follows:

- (1) The quasi-steady state of the electrochemical-cell based on the fluctuation characteristics of oxygen in time domain is proposed. The mortar with 40% pore saturated reaches the quasi-steady state faster than the saturated mortar.
- (2) The development of electrochemical-cell from a non-steady to a quasi-steady state leads to a decline in the half-cell potential, which increases the probability of hydrogen embrittlement.
- (3) The corrosiveness of mortar suffered LSC with 40% pore saturated is much greater than that of saturated mortar. The average corrosion current density in the quasi-steady state is 44.64 mA/m² and 6.67 mA/m², respectively.

CRedit authorship contribution statement

Peng Han: Conceptualization, Data curation, Formal analysis, Investigation, Validation, Visualization, Writing - original draft, Writing-review & editing. **Guofu Qiao:** Funding acquisition, Methodology. **Bingbing Guo:** Resources, Software. **Dongsheng Li:** Project administration. **Jinping Ou:** Supervision.

Declaration of Competing Interest

The authors declare that they have no known competing financial interests or personal relationships that could have appeared to influence the work reported in this paper.

Acknowledgements

This research was supported by grants from the National Key Research and Development Program of China (Project No. 2018YFC0705606, 2017YFC0703410), the Nature Science Foundation of China (NSFC) (Project No. 51578190), the special Fund for the Innovative Talents in the Field of Science and Technology in Harbin (Project No.: RC2014QN012014) and the foundational Research Funds for the Central Universities (Project No.: HIT. BRET III. 2012 33).

References

- [1] Muehlenkamp EB, Koretsky MD, Westall JC. Effect of Moisture on the Spatial Uniformity of Cathodic Protection of Steel in Reinforced Concrete. *Corrosion-US* 2005;6(61):519–33.
- [2] Hong Y, Li Z, Qiao G, Ou J. Numerical simulation and experimental investigation of the stray current corrosion of viaducts in the high-speed rail transit system. *Constr Build Mater* 2017;157:416–23.
- [3] Tang K. Corrosion of steel fibre reinforced concrete (SFRC) subjected to simulated stray direct (DC) interference. *Mater Today Commun* 2019;20:100564.
- [4] Tang K, Wilkinson S. Corrosion resistance of electrified railway tunnels made of steel fibre reinforced concrete. *Constr Build Mater* 2020;230:117006.
- [5] Tang K. Stray current induced corrosion of steel fibre reinforced concrete. *Cement Concrete Res* 2017;100:445–56.
- [6] Ouadah M, Touhami O, Ibtouen R, Benlamouar MF, Zergoug M. Corrosive effects of the electromagnetic induction caused by the high voltage power lines on buried X70 steel pipelines. *Int J Elec Power* 2017;91:34–41.
- [7] Cotton I, Charalambous C, Aylott P, Ernst P. Stray Current Control in DC Mass Transit Systems. *IEEE T Veh Technol* 2005;54(2):722–30.
- [8] Peabody AW, Bianchetti ERL. Peabody's control of pipeline corrosion, 2nd ed.; 2001.
- [9] Charalambous CA, Aylott P. Dynamic Stray Current Evaluations on Cut-and-Cover Sections of DC Metro Systems. *IEEE T Veh Technol* 2014;63(8):3530–8.
- [10] Xu S, Li W, Wang Y. Effects of Vehicle Running Mode on Rail Potential and Stray Current in DC Mass Transit Systems. *IEEE T Veh Technol* 2013;62(8):3569–80.
- [11] Cheung MMS, Cao C. Application of cathodic protection for controlling macrocell corrosion in chloride contaminated RC structures. *Constr Build Mater* 2013;45: 199–207.
- [12] Shi J, Zou Y, Ming J, Wu M. Effect of DC stray current on electrochemical behavior of low-carbon steel and 10%Cr steel in saturated Ca(OH)₂ solution. *Corros Sci* 2020;169:108610.
- [13] Qiao G, Guo B, Ou J. Numerical Simulation to Optimize Impressed Current Cathodic Protection Systems for RC Structures. *J Mater Civil Eng* 2017;29(6): 4017005.
- [14] Guofu Q, Bingbing G, Zuohua Li, et al. Corrosion behavior of a steel bar embedded in a cement-based conductive composite - ScienceDirect. *Constr Build Mater* 2017; 134(Mar. 1):388–96.
- [15] Guo B, Hong Y, Qiao G, Ou J, Li Z. Thermodynamic modeling of the essential physicochemical interactions between the pore solution and the cement hydrates in chloride-contaminated cement-based materials. *J Colloid Interf Sci* 2018;531: 56–63.
- [16] Guo B, Hong Y, Qiao G, Ou J. A COMSOL-PHREEQC interface for modeling the multi-species transport of saturated cement-based materials. *Constr Build Mater* 2018;187:839–53.
- [17] Bertolini L, Carsana M, Pedferri P. Corrosion behaviour of steel in concrete in the presence of stray current. *Corros Sci* 2007;49(3):1056–68.
- [18] Lalvani SB, Lin X. A revised model for predicting corrosion of materials induced by alternating voltages. *Corros Sci* 1996;38(10):1709–19.
- [19] Lalvani SB, Lin XA. A theoretical approach for predicting AC-induced corrosion. *Corros Sci* 1994;36(6):1039–46.
- [20] Tang K. Stray alternating current (AC) induced corrosion of steel fibre reinforced concrete. *Corros Sci* 2019;152:153–71.
- [21] Zhu M, Du CW, Li XG, Liu ZY. Stress Corrosion Cracking of X80 Pipeline Steel Under Various Alternating Current Frequencies in High-pH Carbonate/Bicarbonate Solution. *Corrosion-US* 2014;70(12):1181–8.
- [22] Tzeng Y, Lee C. Analysis of Rail Potential and Stray Currents in a Direct-Current Transit System. *IEEE T Power Deliver* 2010;25(3):1516–25.
- [23] Dolara A, Foiaidelli F, Leva S. Stray Current Effects Mitigation in Subway Tunnels. *IEEE T Power Deliver* 2012;27(4):2304–11.
- [24] Memon SA, Fromme P. Stray Current Corrosion and Mitigation: A synopsis of the technical methods used in dc transit systems. *IEEE Electr Mag* 2014;2(3):22–31.
- [25] Paul D. DC Stray Current in Rail Transit Systems and Cathodic Protection [History]. *IEEE Ind Appl Mag* 2016;22(1):8–13.

- [26] Angst UM, Elsener B, Larsen CK, Vennesland Ø. Chloride induced reinforcement corrosion: Electrochemical monitoring of initiation stage and chloride threshold values. *Corros Sci* 2011;53(4):1451–64.
- [27] Bertolini L, Bolzoni F, Gastaldi M, Pastore T, Pedferri P, Redaelli E. Effects of cathodic prevention on the chloride threshold for steel corrosion in concrete. *Electrochim Acta* 2009;54(5):1452–63.
- [28] Mundra S, Criado M, Bernal SA, Provis JL. Chloride-induced corrosion of steel rebars in simulated pore solutions of alkali-activated concretes. *Cement Concrete Res* 2017;100:385–97.
- [29] Mundra S, Prentice DP, Bernal SA, Provis JL. Modelling chloride transport in alkali-activated slags. *Cement Concrete Res* 2020.
- [30] Huet B, Hostis VL, Santarini G, Feron D, Idrissi H. Steel corrosion in concrete: Determinist modeling of cathodic reaction as a function of water saturation degree. *Corros Sci* 2007;49(4):1918–32.
- [31] Chen Z, Koleva D, van Breugel K. A review on stray current-induced steel corrosion in infrastructure. *Corros Rev* 2017;35(6):397–423.
- [32] Zhang XL, Jiang ZH, Yao ZP, Song Y, Wu ZD. Effects of scan rate on the potentiodynamic polarization curve obtained to determine the Tafel slopes and corrosion current density. *Corros Sci* 2009;51(3):581–7.
- [33] Qiao G, Ou J. Corrosion monitoring of reinforcing steel in cement mortar by EIS and ENA. *Electrochim Acta* 2007;52(28):8008–19.
- [34] Qiao G, Sun G, Hong Y, Qiu Y, Ou J. Remote corrosion monitoring of the RC structures using the electrochemical wireless energy-harvesting sensors and networks. *NDT&E Int* 2011;44(7):583–8.
- [35] Lothenbach B, Kulik DA, Matschei T, Balonis M, Baquerizo L, Dilnesa B, et al. Cemdata18: A chemical thermodynamic database for hydrated Portland cements and alkali-activated materials. *Cement Concrete Res* 2019;115:472–506.